Effects of metallic wire-mesh on flow boiling CHF from the downward-facing heated wall

In Yeop Kang[a], Soonil Kwon[a], Junha Kang[a], Hyungdae Kim[a*]
[a] *Department of Nuclear Engineering, Kyung Hee University, Yong In, Republic of Korea*
E-mail: hdkim@khu.ac.kr

1. Introduction

The IVR (In-vessel corium Retention)-ERVC (External Reactor Vessel Cooling) strategy is an effective method for maintaining reactor vessel integrity during a severe accident in a nuclear power plant [1]. Since the Fukushima nuclear accident in 2011, it became more prominent. Nucleate boiling phenomena at the lower head of the reactor vessel plays a role in the performance of the IVR-ERVC strategy. If the decay heat is excessively generated in the reactor vessel, the critical heat flux (CHF) phenomena can occur on the downward-facing heated wall of the lower head so that integrity of the reactor vessel can be threatened. Therefore, development of the CHF enhancement technique applicable to the downward-facing heated wall of the reactor vessel is desired to improve the cooling performance of the ERVC strategy.

To prove feasibility of the IVR-ERVC strategy, many studies have been performed [2-5]. Recently, diverse CHF enhancement techniques were investigated, including nanofluid, surface modification, microchannel structure and hydrid approaches [6]. The research on nanofluids seems to have reached a mature stage, but the long period stability and maintenance problem, as well as the cleaning process, remain unresolved. Although surface modification has impressive research results, the actual manufacturing process at the large engineering scale for the reactor vessel application is still challenging.

Kim et al. [7] proposed stainless-steel porous wire-meshes to improve CHF without changing the physical or chemical properties of the boiling surface in pool boiling. In the study, it was found that presence of a wire-mesh on a boiling surface inhibited excessive dry spots due to capillary flow along the hydrophilic wires.

The wire-mesh method for CHF enhancement is simpler compared to other ones and can be easily manufactured on a large scale without affecting the fluid characteristics or structural integrity. In this study, the CHF enhancement performance of the wish mesh for application to ERVC was experimentally investigated under flow boiling on a downward-facing heated wall. To examine the underlying physical mechanism of the CHF enhancement mechanism, the dynamics of vapor bubbles and the associated liquid-vapor phase distribution on the boiling surface was visualized using the integrated high speed video camera and infrared (IR) camera.

2. Experimental methods

2.1. Electrochemical etching of wire-mesh

Fig. 1 shows an electrochemical etching process used in this study to fabricate porous hydrophilic structures on wire-meshes. Wire-meshes with 0.5-mm diameter and 1.31-mm opening length were selected. Those were etched using 3.6% HCl and 1.2% HNO_3 solutions diluted in a 1:1 ratio 500 mL Aqua Regia solution. We prepared stainless steel 304 wire-mesh of 12×45 mm^2 as the target. A carbon plate electrode of 15×50 mm^2 was placed parallel to the wire-mesh in 7 cm. During etching, the solution was uniformly mixed using the magnetic stirrer. We calculated the current values based on the total area of each etched wire-mesh. The current density value was 0.857 A/cm^2. After etching, the etched wire meshes were rinsed in deionized water and completely dried before the boiling test.

Interestingly, the etched wire-mesh had hydrophobic Cassie-Baxter properties when completely dried after etching but showed hydrophilic Wenzel properties when wetted.

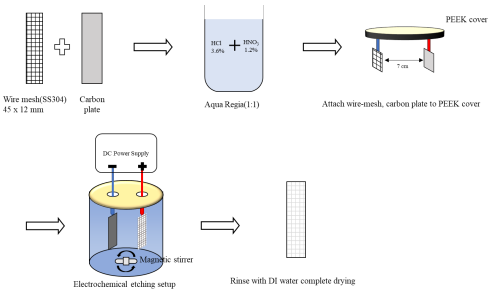

Fig 1. Electrochemical etching process of a wire mesh sample to fabricate porous nanostructures

2.2 Experiment facilities

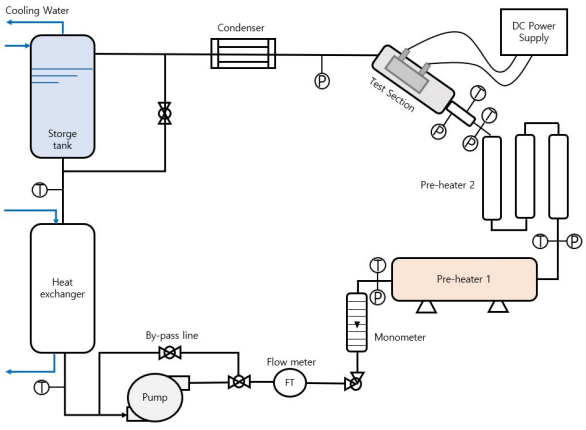

Fig 2. Schematic illustration of test facility

Fig. 2 shows the flow boiling test facility used in this study, which consisted of a rectangle channel, a storage tank, a pre-heater (15 kW), 3 cartridge heater (3 kW), a centrifugal pump (Hydra-cell G10X), a heat exchanger (22 kW) and condenser. Deionized water was used as a working fluid.

The test section comprised rectangle channel with 52 mm × 61 mm sides and 106 mm length. Boiling sample made of silicon wafer was surrounded by PEEK insulator. The other sides comprised polycarbonate windows. The contact angle of deionized water on the silicon wafer was 70.1°. The heater was heated by Joule heating. Degassing process was performed by heating the deionized water (above 97℃) and circulating it for 6 hours.

The estimated mass flow rate of coolant under IVR-ERVC was estimated as 1,200 kg/s from a previous study [8]. Hence, the mass flux was set as 200 kg/m^{2}s corresponding to the value estimated in the actual condition. The subcooling temperature was set to 5 K, the heat flux was from 100 to 800 kW/m^2 and inclination was controlled to 15° and 30°.

2.3 Experiment boiling surface process

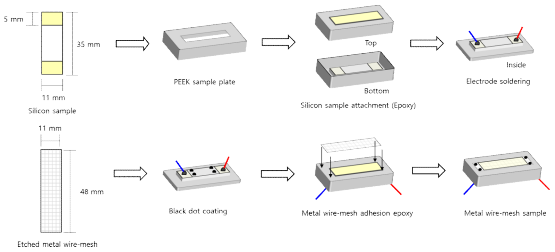

Fig 3. Silicon wafer boiling simple process

Fig. 3 shows a silicon wafer boiling sample process used in this study test section. 500 μm thick silicon wafer was used as the boiling heater material. On the upper surface of the boiling surface, a 2 μm thick silicon dioxide (SiO_2) layer was thermally grown for electrical insulation against the fluid, and on the back surface of the boiling surface, a 100 μm thick Au film and a 10 μm thick Ti film were deposited to from the electrical connection between the boiling heater and the DC power supply.

The silicon wafer sample is partially transparent to photo-graphing spectrum region (λ = 3-5 μm) of the IR camera. Therefore, four black dots of carbon graphite were coated on the back side of the substrate to measure the average temperature of the boiling surface.

The etched wire-mesh and the silicon boiling sample were combined to the PEEK zig using epoxy (Duralco 4538). Then, it was mounted to the test section.

2.4 Image processing

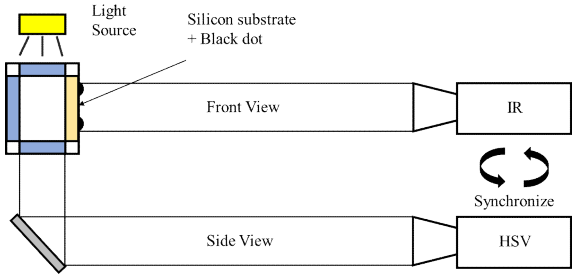

Fig 4. Schematic of the test section set up using IR and high-speed camera

Fig. 4 shows schematic of the test section set up using light source (LLXP150-W), IR (FLIR SC6000) and high-speed camera (Phantom v7.3) used in this study.

We obtained the temperature data from the black dot area and extracted the dry area by decreasing and increasing the temperature due to boiling in areas other than the black dot area via IR camera. Using a function generator (Agilent 33522A), the IR and high-speed camera were simultaneously captured to visualize the boiling phenomenon. The IR camera images were captured at 500 frame per second and high-speed camera images ware captured at 5000 frame per second, synchronized at a ratio of 1:10 and captured images for one second. Fig. 5 shows the sample images from the IR and high-speed camera.

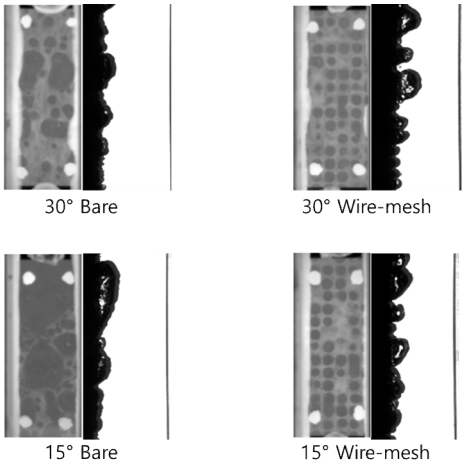

Fig 5. High-speed and IR camera images during flow boiling (conditions were G: 200 kg/m^{2}s, T_{sub}: 5 ℃ and q'': 200 kW/m^2)

3. Result

3.1. Boiling curve

In the boiling curve of Fig. 6, the CHF enhancement in the wire-mesh samples compared to the bare one is clearly observed. While the CHF value of the bare sample were 337.61 kW/m^2 and 543.43 kW/m^2 at 15° and 30°, respectively, the wire-mesh samples showed

the increased CHF values of 425.28 kW/m^2 and 817.66 kW/m^2 correspondingly.

The variation of heat transfer coefficient (HTC) for each boiling sample is shown in Fig. 7. As the inclination decreases, the HTC decreases, which indicates that boiling heat transfer degrades as the orientation of the heating wall approaches toward downward-facing horizontal.

The CHF on the wire-mesh sample surface appeared at the lower wall superheat than that on the bare surface. Due to the lattice structure and inability for the bubbles to escape easily, the HTC was lower at a low heat flux than that of the bare sampled surface.

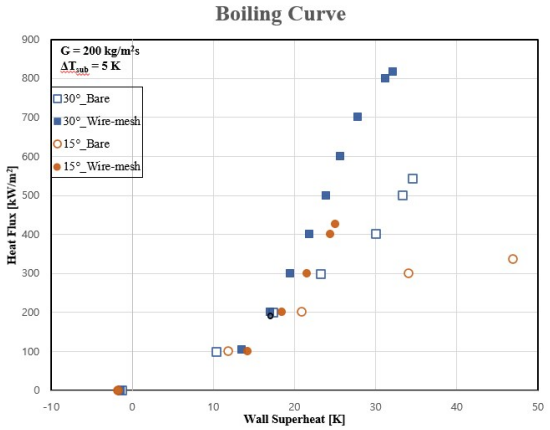

Fig 6. Boiling curve of bare and wire-mesh sample

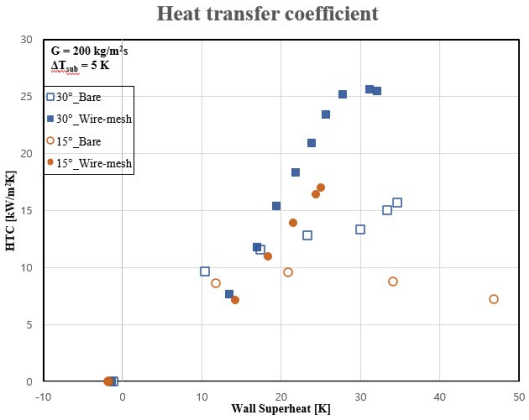

Fig 7. Heat transfer coefficient of bare and wire-mesh sample

3.2. Bubble dynamics

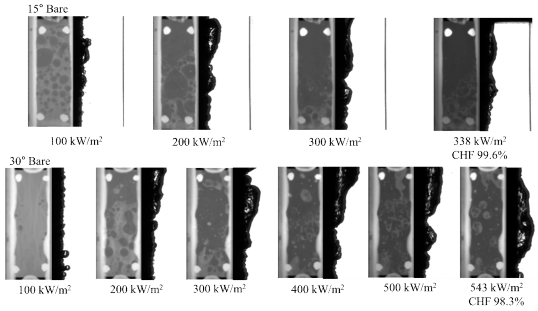

Fig 8. Bubble dynamics and liquid-vapor phase distribution during boiling on the bare sample as a function of heat flux.

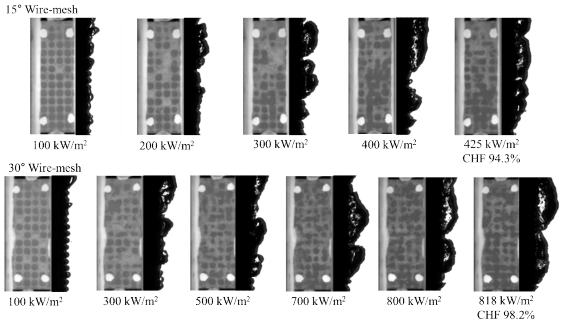

Fig 9. Bubble dynamics and liquid-vapor phase distribution on the wire-mesh sample during boiling as a function of heat flux.

Figs. 8 and 9 show the results of synchronized captured images using IR camera and high-speed camera according to the inclination of the boiling sample. At the inclination of 15° in comparison to 30°, the bubble height decreased, the bubble length increased, and the coverage of the dry area on the boiling surface increased.

By using the wire-mesh grid, the effective surface roughness increases, which increases the frictional drag force on the slug bubble. In addition, the wire-mesh grid prevents bubbles from coalescing. Therefore, the slug bubble length decreases compared to bare boiling samples.

This reduces the HTC by disturbing nucleate boiling heat transfer from the boiling surface. As for the effects of wire-mesh, bubbles are trapped in the grid structure at low heat flux and are distributed to the wire-mesh at regular intervals. Furthermore, it was confirmed that as the heat flux increased, bubbles gradually coalesced together to create single dry spots between the wire-mesh. Slug bubble lift-off decreases the dry spot proportion in comparison to low heat flux.

3.3. Distribution of dry spots

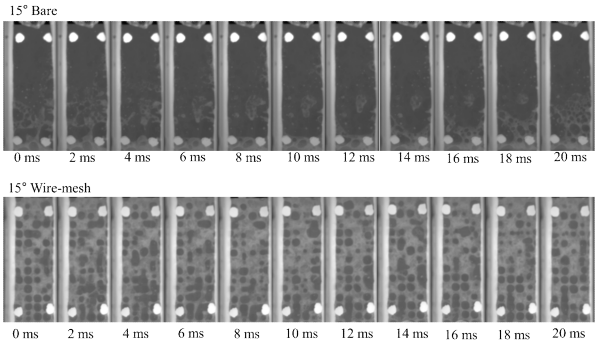

Fig 10. Comparison of phase distribution dynamics on the bare and wire-mesh samples for the downward inclination angle of 15° and q''=300 kW/m^2

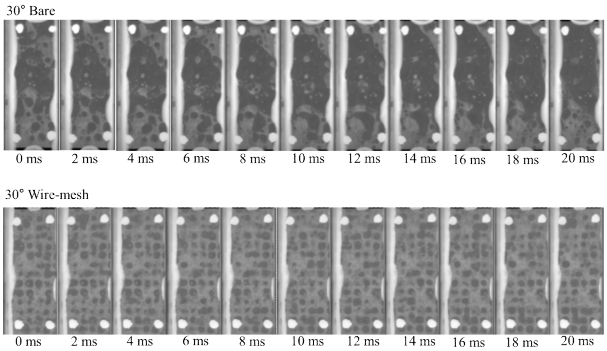

Fig 11. Comparison of phase distribution dynamics on the bare and wire-mesh samples for the downward inclination angle of 30° and q''= 300 kW/m^2

Fig. 10 and 11 show the bubble behavior with time. In contrast to the bare boiling sample, which has a low height and forms a dry spot in a large area once slug bubbles grow over a certain size, bubbles formed on the wire-mesh boiling sample do not spread widely due to the grid on the surface and occupy a certain grid area. Hence, it has a high height (slug bubble) and narrows the dry spot.

At a result, the dry spot occupied before the coalesced bubbles escaped prevents the dry spot from expanding due to inflow of liquid from the side through capillary action (called 'capillary pumping') [7] in the where the wire-mesh grid exists. Moreover, when observing the dry spot of the wire-mesh grid, the coalesced slug bubbles did not cover the entire boiling surface, and the shape of the bubble is confirmed according to the wire-mesh grid structure. This reduces the area the bubbles cover the boiling heating surface, leading to improved CHF. Fig. 12 shows the dry spot ratio by heat flux.

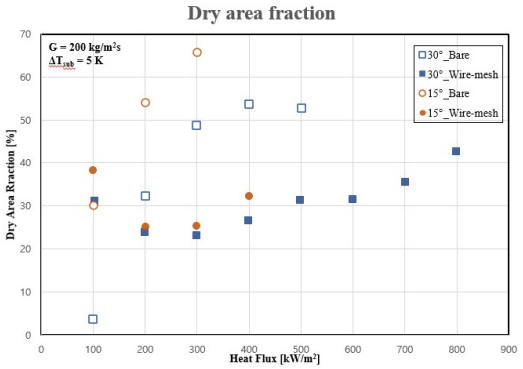

Fig 12 The fraction of dry area as a function of heat flux

4. Summary

To examine the effects of hydrophilic porous wire-mesh on the CHF enhancement for application to IVR-ERVC, flow boiling experiments on the downward-facing heating wall were conducted at the downward inclination angles of 15° and 30°. The experimental study was performed by photographing synchronized wall temperature distribution (IR camera) and bubble behavior (High-speed camera).

It was observed that the critical heat flux of the wire-mesh boiling sample was improved by 33% and 50%, respectively. Heat transfer at the boiling sample surface and the change in the dry spot were analyzed, and the cause of the CHF enhancement was determined based on the bubble behavior.

The experiment study of CHF enhancement using wire-mesh concluded that the slug bubble length had reduced, and that cooling liquid was flowing around the dry spot. The slug bubble on the boiling sample surface to which the wire-mesh is attached decreases in length and increases in height compared to the slug bubble on the bare boiling sample, which reduces the dry spot. By supplying liquid through capillary pumping from the bottom of the wire-mesh grid, the inflow of fluid around the dry spot facilitates the smooth supply of liquid around the dry spot and delays the occurrence of CHF by suppressing the expansion of the dry spot.

ACKNOWLEDGMENTS

This work was supported by National Research Foundation of Korea (NRF) funded by the Korean government (MSIT: Ministry of Science and ICT) (2019M2D2A1A02059364).

REFERENCES

[1] J. L. Rempe, K. Y. Suh, F. B. Cheung & S. B. Kim, "In-Vessel Retention of Molten Corium: Lessons Learned and Outstanding Issues", Nuclear Technology 161, pp. 210-267, 2008.
[2] F. B. Cheung, "Limiting Factors for External Reactor Vessel Cooling", Nuclear Technology 152, pp. 145-161, 2005.

[3] S.D. Park, I.C. Bang, “Flow boiling CHF enhancement in an external reactor vessel cooling (ERVC) channel using graphene oxide nanofluid”, Nuclear Engineering and Design 265, pp. 310-318, 2013.
[4] S.D. Park, I.C. Bang, “CHF enhancement through Pressurized Intermediate Layer in IVR-ERVC Strategy”, Transactions of the Korean Nuclear Society Spring Meeting. Jeju, Korea, May 29-30, 2014.
[5] S.L. Song, S.H Chang, “An experimental study on CHF enhancement of wire nets covered surface in R-134a flow boiling under high pressure and high mass flux conditions”, International Journal of Heat and Mass Transfer 90, pp 761-768, 2015.
[6] S. Xie, M.S Beni, J. Cai, J. Zhao, “Review of critical-heat-flux enhancement method”, International Journal of Heat and Mass Transfer 122, pp. 275-289, 2018.
[7] H.D Kim, Y.J Park, H.M Kim, C. Lee, D.W. Jerng, D.E. Kim, “Critical heat flux enhancement by single-layered metal wire mesh with micro and nano-sized pore structure”, International Journal of Heat and Mass Transfer 115, pp. 439-449, 2017.
[8] P.J. Park, K.S Ha, H.Y. Kim, “Detailed Evaluation of Natural Circulation mass flow rate in the Annular Gap between the Outer Reactor Vessel Wall and Insulation under IVR-ERVC”, Annals of Nuclear Energy 89, 50-55, 2016.